

# AUTOMATIC CALCULATION OF BAND DIAGRAMS OF PHOTONIC CRYSTALS USING THE MULTIPLE MULTIPOLE METHOD

Jasmin Smajic, Christian Hafner, Daniel Erni  
Laboratory for Electromagnetic Fields and Microwave Electronics  
Swiss Federal Institute of Technology  
ETH-Zentrum, Gloriastrasse 35, CH-8092 Zürich, Switzerland  
E-mail: [jsmajic@ifh.ee.ethz.ch](mailto:jsmajic@ifh.ee.ethz.ch)

**ABSTRACT** – In the framework of photonic crystal's band structure calculations, we present a novel way – based on several advanced techniques for searching and tracing eigenvalues with the multiple multipole program – to compute these diagrams automatically, efficiently, and with a high accuracy. Finally, we validate the results for some well known test cases.

**Keywords** – band diagram; multiple multipole program; photonic crystal; eigenvalue analysis.

## I. INTRODUCTION

PHOTONIC Crystals (PhCs) were proposed in 1987 by E. Yablonovitch [1] at the University of California, as an optical counterpart to semiconductors, i.e., PhCs should provide a photonic bandgap in the same way that a semiconductor possesses an electronic bandgap. In fact, PhCs are rarely found in nature. Exceptions are opals and butterfly wings. However, thanks to nano-technology it has become possible to fabricate artificial PhCs in the last decade. These PhCs essentially consist of a periodic assembly of dielectric scatterers, i.e., there is a strong link to the well-known structures of grating theory. One of the important differences between PhCs and semiconductors is the size of the unit cell. For a semiconductor, one has a 3D grid consisting of identical atoms, i.e., the lattice constant in all three directions of the crystal is in the order of the diameter of an atom, whereas the cell size of a PhC is in the order of half an optical wavelength, i.e., much larger. From this fact, one expects that the Photonic Integrated Circuits (PICs) based on PhC concept must be much larger than the traditional semiconductor ICs. But – because of the macroscopic size of the PhC's unit cell – one has much more freedom in introducing and fabricating defects in a PhC than in a semiconductor. Note that a semiconductor becomes interesting from the technological point of view only when a few impurities or defects are introduced and the same holds for PhCs. Doping traditional semiconductors is a rather statistical way of introducing defect atoms in a semiconductor and therefore, the building blocks of semiconductor are relatively large blocks of material with a specific doping. These blocks obviously consist of many atoms. When designing a "doped" PhC, one can precisely position and fabricate all defects with a high degree

of freedom – at least it is expected that this can be done in the near future [2].

Although the variety of PhC structures that might be fabricated one day seems to be almost infinite and although many interesting structures were already proposed (various types of waveguides, sharp bends in waveguides without any reflection, couplers, resonators, etc.) or even fabricated on a prototype level, one currently cannot say what kind of PhC structures will be favored. At the moment, one can neither know the materials that are best suited for PhCs – it is well known that a large dielectric contrast is required for obtaining a bandgap, which somehow limits the materials that may be used, but there is no unique choice at all – nor what kind of geometry (2D crystals or 3D crystals [3-5], symmetry, shape of the scatterers) is most appropriate. Thus, there is a strong need for theoretical investigations and simulations of potential structures. The first step of such investigations consists in the computation of the band diagrams of perfect PhCs without any defects. The goal is to find structures that may easily be fabricated and exhibit a broad band gap, i.e., a frequency range where no electromagnetic waves are allowed to propagate within the crystal. In order to find the band gap, one must compute the band diagram of the lowest order modes of the PhC. This is essentially an eigenvalue problem that exhibits several special cases that may cause difficult numerical problems, especially when one is designing a procedure for the automatic, efficient, accurate, and reliable computation of the complete band diagrams for arbitrary structures.

Currently, the most frequently used approach is the Plane Wave Method (PWM) that mainly approximates the electromagnetic field by a superposition of plane waves [6-10]. It is well known, that this method has a problematic convergence [11-13, 10]. Other methods that were used for PhCs are the Finite Difference Time Domain (FDTD) [14,15], the transfer matrix method [16], the Finite Element Method (FEM) [17], and the Boundary Element Method (BEM) [18]. In the following, we apply the latest version of the Multiple Multipole Program (MMP) [19] implemented in the MaX-1 software [20].

In order to obtain efficient, reliable, and accurate results, we carefully analyze the numerical problems that may occur and introduce several new techniques. For reasons of simplicity we focus on the 2D case.

The remainder of the paper is organized as follows: A commonly used representation of PhCs in terms of their band diagram is elucidated in Section II. In Section III we briefly explain the core of our photonic crystal calculations, when MMP is considered. The proper framework of the eigenvalue search is reported in Section IV, whereas in Section V a successful automation of such search procedure is proposed. A validation of our band structure calculation by means of various test examples is given in Section VI. And finally, we conclude this contribution with a short summary in Section VII.

## II. DEFINITION OF THE BAND DIAGRAM

As an introductory example let us consider the simple case of a 2D PhC consisting of dielectric rods arranged in a square lattice and embedded in, e.g., air. For periodic structures it is possible to apply some fundamental theorems from solid state physics. The original lattice for this crystal is given on the left hand side of Fig. 1. For the dielectric constant we can write  $\varepsilon(\vec{r}) = \varepsilon(\vec{r} + \vec{R})$  where  $\vec{R}$  is one of the original lattice vectors. According to Bloch's theorem [6, 7] for the modal field inside the crystal we write:

$$\vec{E} = \vec{E}_{\vec{k}n}(\vec{r}) = \vec{u}_{\vec{k}n}(\vec{r}) \cdot e^{i\vec{k}\cdot\vec{r}} \quad (1)$$

$$\vec{u}_{\vec{k}n}(\vec{r}) = \vec{u}_{\vec{k}n}(\vec{r} + \vec{R}) \quad (2)$$

Note that (1) holds not only for the electric but also for the magnetic field. Bloch's theorem may be proven in classical electro-dynamics [6]. Important consequences of this theorem are [6, 7]:

1.  $e^{i\vec{k}\cdot\vec{R}} = 1$ , i.e.,  $\vec{k}\cdot\vec{R} = N \cdot 2\pi$ , where  $N$  is an integer – the wave vector space (reciprocal space) is discrete,
2.  $\vec{E}_{\vec{k},n}(\vec{r}) = \vec{E}_{\vec{k}+\vec{G},n}(\vec{r})$ , i.e., the reciprocal space is periodic.  $\vec{G}$  is one of the reciprocal lattice vectors.

This allows us to define the so-called reciprocal lattice space, spanned by the reciprocal lattice vectors. We first define the original lattice vectors as follows:

$$\vec{R} = \eta_1 \vec{e}_1 + \eta_2 \vec{e}_2 + \eta_3 \vec{e}_3 \quad (3)$$

where  $\vec{e}_1$ ,  $\vec{e}_2$ ,  $\vec{e}_3$  are three independent lattice vectors and  $\eta_1$ ,  $\eta_2$ ,  $\eta_3$  are integer numbers. Note that  $\vec{e}_3$  is missing in 2D crystals. Similarly, we write for the primitive reciprocal lattice vectors:

$$\vec{G} = \kappa_1 \vec{f}_1 + \kappa_2 \vec{f}_2 + \kappa_3 \vec{f}_3 \quad (4)$$

If we want to construct the reciprocal lattice, we can use [7]:

$$\vec{f}_1 = 2\pi \frac{\vec{e}_2 \times \vec{e}_3}{\vec{e}_1 \cdot (\vec{e}_2 \times \vec{e}_3)}, \quad \vec{f}_2 = 2\pi \frac{\vec{e}_3 \times \vec{e}_1}{\vec{e}_1 \cdot (\vec{e}_2 \times \vec{e}_3)}, \quad \vec{f}_3 = 2\pi \frac{\vec{e}_1 \times \vec{e}_2}{\vec{e}_1 \cdot (\vec{e}_2 \times \vec{e}_3)}$$

These equations are derived from the definition of the reciprocal lattice vector space. For 2D crystals (cylindrical geometry), the vector  $\vec{f}_3$  is omitted and the vector  $\vec{e}_3$  is the unit vector  $\vec{e}_z$  along the cylinder axis.

From the equations above, we can conclude that the discrete translational symmetry of a photonic crystal leads to the fact that modes with the wave vector  $\vec{k}$  and modes with the wave vector  $\vec{k} + \vec{G}$  are identical, i.e., we have periodicity also in the reciprocal space. A special representation of the primitive cell for this periodicity is called the first Brillouin zone (1<sup>st</sup> BZ). It can be defined as a zone around any lattice point in the reciprocal space with points that are closer to this lattice point than to any other lattice point.

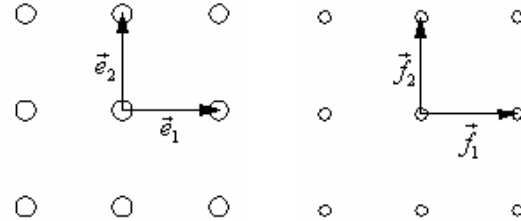


Fig. 1: The original (left) and reciprocal (right) lattice for a 2D photonic crystal (square lattice). Construction details for reciprocal lattice are given in the text.

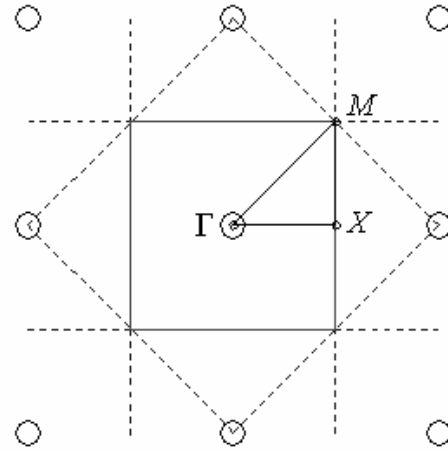


Fig. 2: Construction of the 1<sup>st</sup> Brillouin zone (solid square), its irreducible part (triangle  $\Gamma$ -X-M) and characteristic points for band structure computation ( $\Gamma$ , X, and M).

The Brillouin zone construction (using Bragg's planes – dashed lines) for the square lattice is shown in Fig. 2. Because of the high degree of symmetry, we need to analyze only a small part of the 1<sup>st</sup> BZ. This part is called the *irreducible BZ* (IBZ), [6, 7]. In the case of periodic structures,

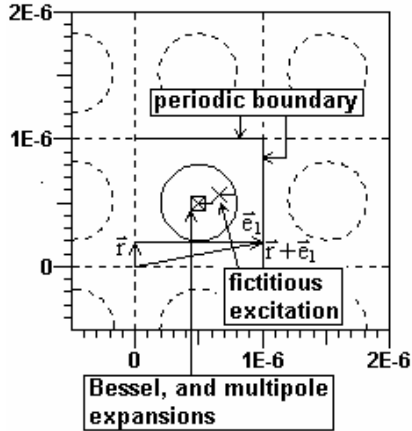


Fig. 3: The unit cell of the photonic crystal with dielectric rods arranged on a square lattice.

it is sufficient to perform the modal field analysis in the area of the IBZ. As illustrated in Fig. 2 the IBZ for a square lattice is a triangle with the corners  $\Gamma$ , X, and M. Since the maxima and minima of the eigenvalues (resonance frequencies) are supposed to be on the borders of the IBZ, it is sufficient to trace the eigenvalues along the sides of the IBZ in order to get the photonic bandgaps. Therefore, the standard band diagram consists of three sections:  $\Gamma$ -X, X-M, and M- $\Gamma$  (see Fig. 5). For other lattices, the procedure is essentially the same [21, 22]. Assume that an arbitrary point in the reciprocal space is considered. This point essentially defines a wave vector. For the periodicity of (3) we then obtain for the field in the original space:

$$\vec{F}(\vec{r} + \vec{R}) = \vec{F}(\vec{r}) \cdot e^{i\vec{k}\cdot\vec{R}} = \vec{F}(\vec{r}) \cdot e^{i(C_1 n_1 |\vec{k}_1| + C_2 n_2 |\vec{k}_2|)} \quad (5)$$

where  $F$  stands for the electric as well as for the magnetic field. In the MMP implementation of the periodic boundary problem  $C_1$ ,  $C_2$  are parameters that characterize the point in the reciprocal lattice space. As a consequence, it is sufficient to know the field in a unit cell (as an equivalent representation of the primitive cell) of the original space. Let us call this the original cell. Note that neither the shape nor the location of the original cell is unique, but for both the square and the hexagonal lattice we may simply use quadrangular original cells as shown in Fig. 3 and 4.

For the square lattice, the relation between the periodic constants ( $C_1$ ,  $C_2$ ) and the position in the IBZ is very straight forward, i.e., these are the Cartesian components ( $C_x$ ,  $C_y$ ) of the wave vector  $\vec{k}$ . For the hexagonal lattice, the situation is a bit more complicated [23-25].

### III. THE MMP SOLUTION OF PERIODIC PROBLEMS WITH FICTITIOUS BOUNDARIES

Any software for computing band diagrams must handle both eigenvalue problems and periodic structures. The MMP implementation of MaX-1 contains a simple concept for handling arbitrary periodic structures: First, the structure is

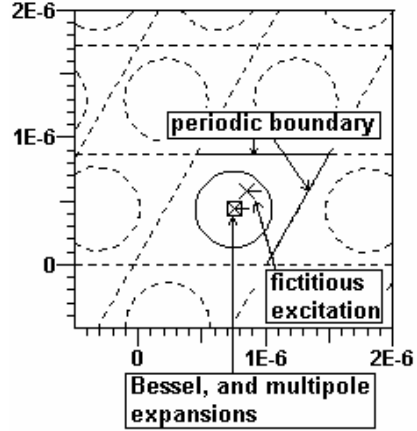


Fig. 4: The unit cell of the photonic crystal with dielectric rods arranged on a hexagonal lattice.

subdivided into cells by an appropriate grid of fictitious boundaries (dashed lines in Fig. 3 and Fig. 4). Assume that the field in one of the infinitely many cells is known, then, the field in all other cells is easily obtained from the periodicity conditions (5), i.e., the Floquet theorem [7].

The geometric shape of the original cell depends on the crystallographic structure (i.e. the crystal symmetry), but it is not unique for a given crystallographic structure at all, because the fictitious boundaries we have introduced, are quite ambiguous. For example, in Fig. 3 we used straight lines between the circular rods. We could replace these lines by curved, periodic lines and we could move these lines to any other position in space. Since we will impose so-called periodic boundary conditions along the fictitious boundaries of the original cell, we have to minimize the numerical problems when we select the fictitious boundaries in such a way that the electromagnetic field along them is as well behaved as possible. Therefore, straight lines in the middle between neighbor rods are most reasonable when the rods are circular or rectangular. When the geometric shape of the rods is more complicated, it may be advantageous to use curved lines.

Once, the original cell is isolated by introducing fictitious boundaries, we can derive boundary conditions for the field along them. In 2D PhCs, the original cell is bounded by two pairs of parallel lines. For example, when  $\vec{r}$  is a point on the left border of the original cell in Fig. 3,  $\vec{r} + \vec{e}_1$  is the corresponding point on the right border, where  $\vec{e}_1$  corresponds to one of the primitive lattice vectors. Because of the periodicity, we obtain from (5):

$$\vec{F}(\vec{r} + \vec{e}_1) = \vec{F}(\vec{r}) \cdot e^{i(C_1 |\vec{k}_1|)} \quad (5')$$

This condition holds for both the electric and the magnetic field in every point along the right boundary of the original cell. We call this the periodic boundary condition that is imposed on the right border of the original cell. Similarly, we can introduce a periodic boundary condition for the upper border.

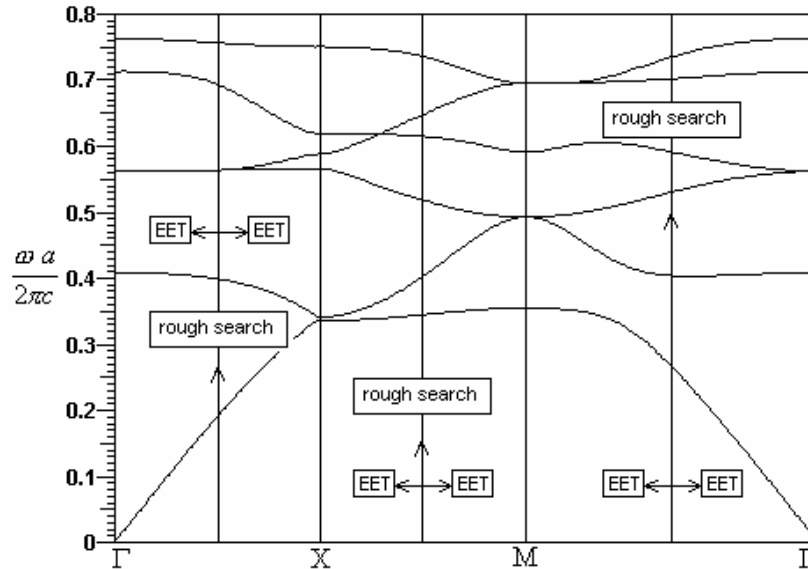


Fig. 5: The band diagram of the photonic crystal with dielectric rods on a square lattice (for H-polarization). The algorithms used within the eigenvalue search procedure are labeled correspondingly.

Having defined the original cell and its periodic boundary conditions, one has to set up the MMP model of the scattering body in the lattice point: We approximate the field in each domain by a superposition of multipole expansions and sometimes by additional, analytic solutions of Maxwell's equations (in the frequency domain). The amplitudes or parameters of the resulting series expansions are then computed with the generalized point matching technique, i.e., by minimizing a weighted error function defined along all natural and fictitious boundaries. For example, for the simple geometry in Fig. 4 we use the following expansions:

$$E_z = \sum_{n=0}^N A_n^E J_n(\kappa r) \cos(n\varphi) + B_n^E J_n(\kappa r) \sin(n\varphi) \quad (6)$$

$$H_z = \sum_{n=0}^N A_n^H J_n(\kappa r) \cos(n\varphi) + B_n^H J_n(\kappa r) \sin(n\varphi) \quad (7)$$

$$E_z = \sum_{n=0}^N C_n^E H_n^1(\kappa r) \cos(n\varphi) + D_n^E H_n^1(\kappa r) \sin(n\varphi) \quad (8)$$

$$H_z = \sum_{n=0}^N C_n^H H_n^1(\kappa r) \cos(n\varphi) + D_n^H H_n^1(\kappa r) \sin(n\varphi) \quad (9)$$

where  $J_n$  is Bessel function of order  $n$ ,  $H_n^1$  is Hankel function of first kind and order  $n$ ,  $\kappa$  is transverse propagation constant and  $(r, \varphi)$  are polar coordinates with respect to the origin at the position of the corresponding expansion. Expansion (6) (Bessel expansion) is used in the case of E-polarization and expansion (7) is used in the case of H-polarization. These Bessel expansions are used for the domain inside of the dielectric rod because these functions have no singularity at origin. Furthermore, these expansions are sufficient because the domain is simply connected. The background domain is not simply connected, because it contains a hole. Therefore,

we need at least two different expansions, namely a multipole expansion (8) or (9) and Bessel expansion (6) or (7). Note that the multipole expansion essentially accounts for the field scattered at the inner boundary, whereas the Bessel expansion accounts for the outer, fictitious boundaries. This means that the Bessel expansion simulates the field that comes from all rods outside the original cell. According to Vekua [24], our set of expansions is complete in the sense that the error of the field is below an arbitrarily small value  $\varepsilon$  provided that the highest orders are big enough and provided that the amplitudes ( $A, B, C, D$  in (6)-(9)) are computed correctly.

#### IV. THE MMP-MAS EIGENVALUE SOLVER

For obtaining the band diagram of a PhC, it is necessary to solve an eigenvalue problem, because there is no excitation like in scattering problems. This means that we only obtain non-trivial solutions (i.e. frequencies) for an arbitrary point of the IBZ (i.e., for a given set of complex values  $C_1, C_2$ ). Thus, we essentially have a periodic resonator problem to solve. The search of resonance frequencies in the MMP code MaX-1 is somehow different from many other numerical methods because MMP uses a full rectangular system matrix obtained from the generalized point matching technique. For such type of matrix it is very demanding to obtain accurate results while avoiding problems with the condition number [25]. Note that condition number problems are especially crucial when one is solving eigenvalue problems. If this is not properly done, one can obtain a "noisy" behavior near the eigenvalues and this can heavily disturb the numerical eigenvalue search procedures. However, the standard MMP eigenvalue search procedure first defines a real valued, positive eigenvalue search function

$$\eta(e) = \frac{\|E(e)\|^2}{A^2(e)} \quad (10)$$

where  $e$  is the eigenvalue (i.e. the resonance frequency),  $E$  is the weighted residual, and  $A$  is an amplitude that may be retrieved from any field component in a specific test point (or an integral over some field profile). For the band gap computation, it is most reasonable to define  $A^2$  as the total electromagnetic energy within the original cell. According to (10) the desired eigenvalues are characterized by the minima of the search function  $\eta$ . Analyzing the shape of  $\eta$  near the minima provides additional information on the accuracy of the solution.

Although more reliable results are obtained when the

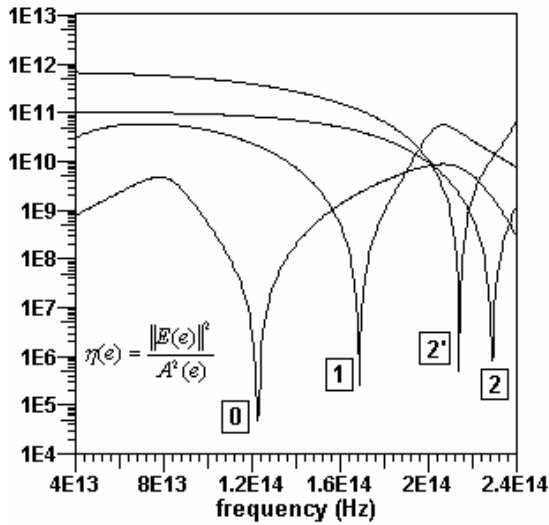


Fig. 6: The behavior of the eigenvalue search function (in the  $\Gamma$  point) of one single model with four different "last" expansions (the order of the last expansion is labelled in the figure)

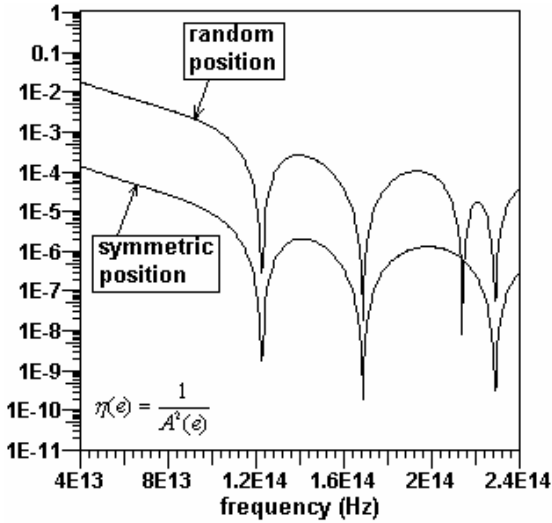


Fig. 7: The behavior of the eigenvalue search function (for a  $k$ -vector in the  $\Gamma$  point) using the fictitious excitation in a random and symmetric position respectively.

amplitude is defined by an appropriate integral, the definition in one or a few test points is sufficient for most cases. Since the numerical intergration may be time-consuming, one usually prefers the simpler test point method. However, it is important to note that the definition of the search function is not unique. By defining different search functions, one can gain even more intrinsic information providing a good error estimation and for validation purposes. As depicted in Fig. 6, even for a single model (fixed amplitude definition and fixed multipole expansion), one can address the different minima of the same eigenvalue search functions simply by rearranging the columns of the MMP matrix. In fact, in the Givens update algorithm [25], which was used for solving the MMP matrix equation, the last expansion somehow plays the role of an excitation. When it happens that the spatial symmetry of such excitation is not contained in the symmetry of the searched eigenmode, this mode will not be "excited", hence, the corresponding minimum of the eigen-value search function is suppressed. Although, it may be desirable to suppress some modes in applications where not all modes must be considered, this is usually inconvenient for the automatic computation of the complete band structure. We therefore look for an alternative technique.

Remember that we have introduced fictitious boundaries for handling the periodic problem. Similarly, we now can introduce a fictitious excitation that is defined in such a way that all modes are excited (Fig. 7). This concept mimics the measurement of resonance frequencies, where one always needs an excitation of the resonator and a test point (or port) where the signal is measured. By sweeping the frequency of the excitation, the peaks of the amplitude  $A$  in the test point can be readily assigned to the resonance frequencies of the different modes. This procedure was first introduced by the Method of Auxiliary Sources (MAS) [26] and a similar method was used by Sakoda [27]. Finally, the method was adapted to MMP by Moreno [28]. MAS uses eigenvalue

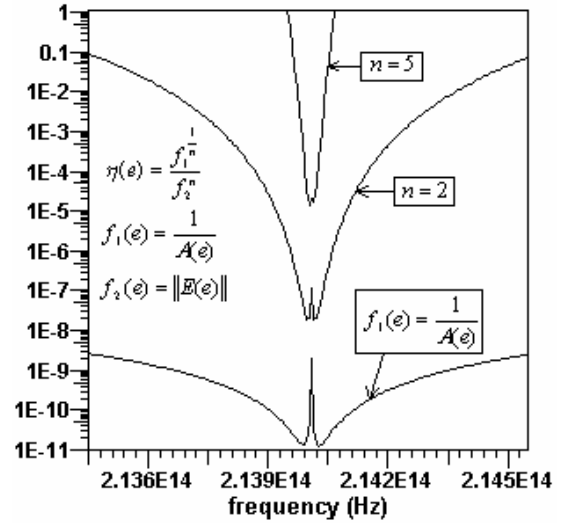


Fig. 8: The "twin minima" phenomenon, behavior of the eigenvalue search function within the eigenvalue search procedure using a randomly located fictitious excitation.

search functions  $\mu$  such as the energy density  $A^2$  at the test point are used. The eigenvalues are then obtained from the maxima of  $\mu$ . The analysis of  $\mu$  near the maxima has yielded a strange "double peak" phenomenon that disturbs the numerical search procedure. The standard MMP-MAS eigenvalue solver searches for minima of the eigenvalue search function  $\eta = 1/\mu = 1/A^2$ , i.e., one obtains "twin minima" instead of double peaks, as shown in Fig. 8. The "double peak" phenomenon and the "twin minima" are caused by a very sharp peak of the residual  $E$  at the correct eigenvalue position. Note that this peak is not obtained in the standard MMP approach without fictitious excitations. Of course, the residual peak may also be used for defining the eigenvalues. Since these peaks are extremely sharp, it is very likely that one of the eigenvalues is missed by the rough search routine that searches for all eigenvalues. In order to overcome these problems, one can define more complicated eigenvalue search functions  $\eta$  as proposed in Fig. 8. This allows one to suppress the double peak phenomenon. Unfortunately, one may encounter numerical underflow problems in some applications. Therefore, the current MaX-1 eigenvalue solvers

uses three different "competing" eigenvalue search functions: 1) A complicated one with user-definable exponent  $n$ , 2) the inverse of the amplitude, and 3) the proper residual. Using all of these three functions, the code is capable to detect the correct locations of the eigenvalues. An alternative to overcome the twin minima problems is the introduction of "fictitious losses" that smoothen the resulting search function  $\eta$ .

Since one often considers a broad frequency range, it is not reasonable to find the eigenvalues by plotting the eigenvalue search function over the entire range with a very high resolution. It is much more efficient to subdivide the search process into two steps: 1) Rough detection of all eigenvalues and 2) fine search, i.e., accurate computation of the eigenvalues. The first step seems to be trivial as soon as the problems mentioned above have been solved. The second step requires a fast minimum search procedure for real functions. The algorithm used in MaX-1 is mainly based on a parabolic interpolation because the search function near the minima is usually almost parabolic – provided that the double peak phenomenon has been removed.

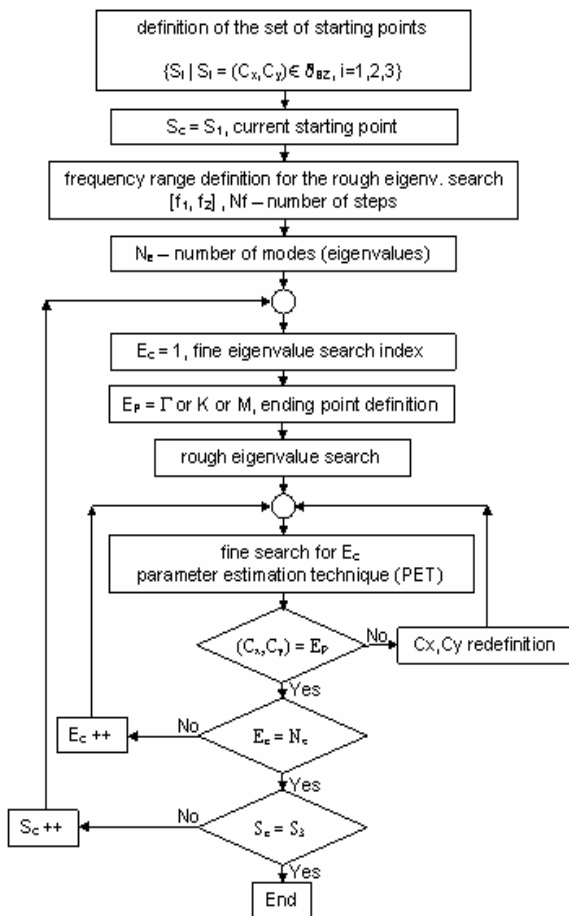


Fig. 9: The algorithm for the band structure computation using MMP.

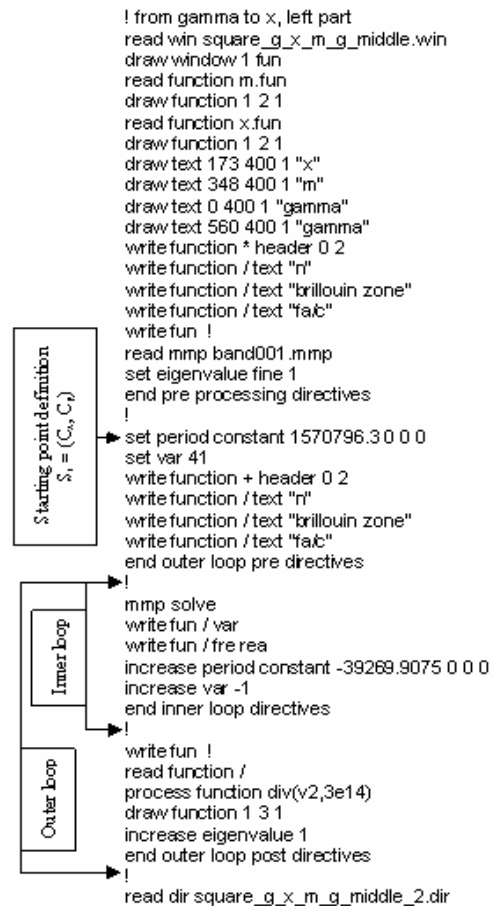


Fig. 10: The algorithm for band diagram computation written in the MaX-1 script language.

TABLE I  
CONVERGENCE CHARACTERISTICS, COMPUTATION FOR 1<sup>ST</sup> AND 6<sup>TH</sup> EIGENFREQUENCY AT X POINT OF IBZ

Number of unknowns	Eigenfrequency 1			Eigenfrequency 6		
	Frequency (Hz)	Error (%)	Field mismatch. (%)	Frequency (Hz)	Error (%)	Field mismatch. (%)
20	1.0223585e14	1.473	9.620748e-0	2.3465308e14	4.194	2.306028e+1
36	1.0095955e14	0.206	4.204639e-0	2.2567438e14	0.207	4.449937e+0
52	1.0078338e14	0.032	0.288115e-0	2.2512072e14	0.039	0.824365e-0
94	1.0074678e14	0.005	4.465747e-2	2.2519421e14	0.006	0.128581e-0
164	1.0075153e14	0.000	4.729721e-7	2.2520785e14	0.000	3.551224e-6

Having a closer look to typical band diagrams (Fig. 3), we see different situations which can cause problems for both the rough search and the fine search. Mainly at the  $\Gamma$  and the M point we usually observe degenerate modes. Furthermore, we have areas with almost degenerate modes and points where different lines seem to cross each other, where the modes are (accidentally) degenerated. When the rough search is performed to degenerate points, it usually cannot detect all modes involved. Even if the search procedure is started in a close vicinity to such degeneracies, it will be too time-consuming to iterate into all eigenmodes. In order to overcome these problems, it is reasonable to start a rough search in a domain where all eigenvalues could be easily tracked down (e.g. the interval between  $\Gamma$  and X in the band diagram of Fig. 5). Once this has been done, one can trace each eigenvalue by moving a small step either to the left or right side within the band diagram, and repeating this

procedure until the border of the diagram is reached. For each such step, only a fine search must be performed. Depending on 1) the desired accuracy, 2) the step size, and 3) special properties of the model, several iterations are required. The number of iterations could be drastically reduced when using the Eigenvalue Estimation Technique (EET) implemented in MaX-1 [19]. This technique uses the information of previous eigenvalue solutions for the extrapolation of the current eigenvalue's search interval. Typically, 4–12 iterations per step are sufficient for obtaining an eigenvalue with a high precision. For example, for tracing the first mode in Fig. 3, 280 search steps were performed and 5 iterations per step were required in the average.

V. AUTOMATIC EIGENVALUE SEARCH

Referring to e.g. Fig. 5 a standard band diagram consists of three different intervals corresponding to the three sides of

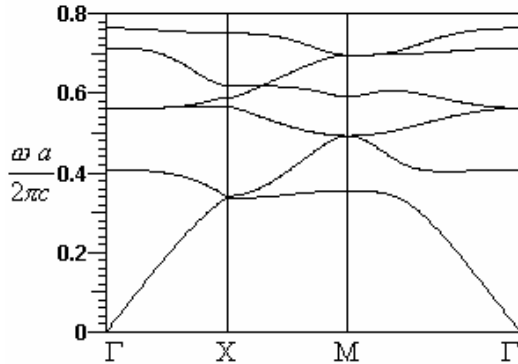


Fig. 11: The band diagram of the photonic crystal with dielectric rods and square lattice, H-polarization, the first 6 modes.

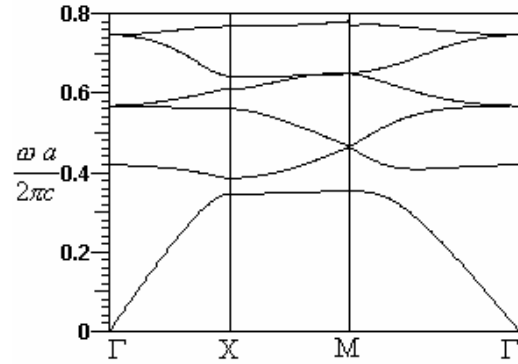


Fig. 13: The band diagram of the photonic crystal with dielectric rods and hexagonal lattice, H-polarization, the first 6 modes.

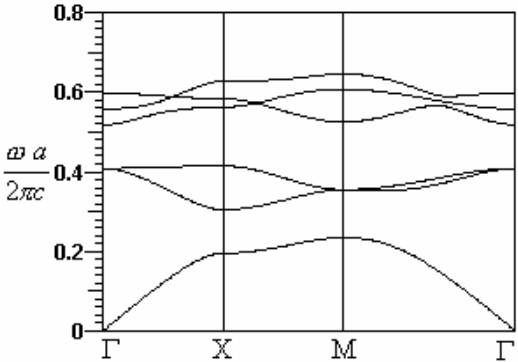


Fig. 12: The band diagram of the photonic crystal with dielectric rods and square lattice, E-polarization, the first 6 modes.

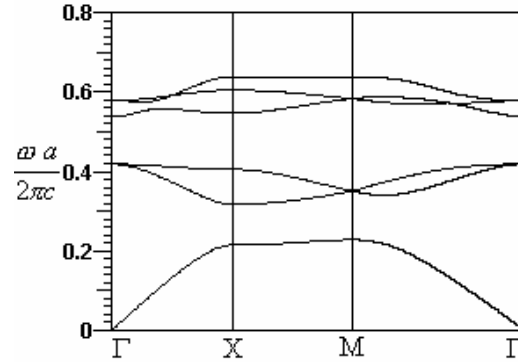


Fig. 14: The band diagram of the photonic crystal with dielectric rods and hexagonal lattice, E-polarization, the first 6 modes.

the IBZ. When the rough search is started somewhere in the middle of such an interval (e.g. in the area between  $\Gamma$  and X in the band diagram), it must be repeated three times. After each rough search the fine search must be repeated for each obtained eigenvalue and, finally, the fine search routine must run for each eigenvalue once towards the left and once towards the right side of the band diagram, as depicted in Fig. 5. MaX-1 contains a script language that allows one to define complicated procedures such as the search procedure mentioned above. The set of MaX-1 directives for the automatic generation of a band diagram from the point in the middle between  $\Gamma$  and X to the  $\Gamma$  point, is given in Fig. 10, and the complete algorithm for this procedure is given in Fig. 9. It is obvious that the algorithm is not simple and the overall procedure relies on fast computer resources.

## VI. NUMERICAL VERIFICATION

We have applied MMP to various PhC lattices. Internal tests show excellent convergence. Therefore high accuracy may easily be obtained. Table I shows the MMP estimate of the mismatching errors along the boundary for the model outlined in Fig. 3 with different maximum orders of the multipoles and Bessel expansions, i.e., with different numbers of unknowns. Note that the computation time typically is proportional to the cube of the number of unknowns because we use a brute-force full matrix solver (Givens update scheme). Despite of this, the computation time remains reasonably short because the matrices obviously are much smaller than the matrices used in other methods. For example Fig. 11 was obtained with 3 rough-search routines, 100 frequency steps each. The total number of 1656 plotted points required were then computed with 8280 MMP evaluations of  $\eta$ , i.e. approximately 5 iterations per point in the diagram were performed. The total calculation time was 40 minutes on a Pentium 4, 2GHz. Because of the excellent convergence, we also can estimate the accuracy of the eigenvalues by comparing them with a very accurate MMP model. As one can see from Table I, one only obtains one more digit when doubling the number of unknowns.

In order to validate this algorithm, several calculations were performed and results were compared with the results of MPB package developed at the MIT [29]. For the PhC with square lattice and dielectric rods (Fig. 3), a band diagram calculation was performed for different field polarizations and the results are given in Fig. 11 (H-polarization) and Fig. 12 (E-polarization). The results for the hexagonal lattice case (Fig. 4), are depicted in Fig. 13 (H-polarization) and Fig. 14 (E-polarization). These two types of PhC rely on the same lattice data: A dielectric rod with radius  $r=0.3a$  and a dielectric constant of  $\epsilon=11.56$ , the lattice is embedded in air and the lattice constant is  $a=10^{-6}(m)$ . From Figs. 11–14 we deduce a perfect agreement with the MPB results documented in [29].

## VII. CONCLUSION

We have presented an efficient method for band structure calculation for 2D dielectric PhCs. In this framework a fully

automatic algorithm was developed and evaluated along several examples. The eigenvalue searching procedure in the frequency domain has been performed using a fictitious excitation. Optimal eigenvalue search functions have been found while evaluating the total eigenvalue spectrum for  $k$ -values at three preferable points on the IBZ. The three resulting sets of eigenvalues are evolved into a full band diagram using a highly efficient Eigenvalue Estimation Technique (EET). The overall algorithm performs photonic band diagram calculations at a very high level of accuracy and at reasonable computational costs. This algorithm is easily extendable for applications involving localized defect mode analysis [30], various PhC defect waveguide types (supercell approach [31]) and photonic waveguide discontinuities [31], as well.

## ACKNOWLEDGMENT

This work was supported by the Swiss National Science Foundation in the framework of the project NFP-2000-065102.01/1 and the research initiative NCCR Quantum Photonics.

## REFERENCES

- [1] E. Yablanovich, "Inhibited spontaneous emission in solid-state physics and electronics", *Phys. Rev. Lett.*, **58**, pp. 2059-2062, 1987.
- [2] J. Mills, "Photonic crystals head toward the marketplace", Nov. 2002, <http://optics.org/articles/ole/7/11/1/1>.
- [3] K. Busch, S. John, "Liquid-crystal photonic-band-gap materials: the tunable electromagnetic vacuum", *Phys. Rev. Letters*, **83**, pp. 967-970, 1990.
- [4] A. Figotin, Y. A. Godin, "two-dimensional tunable photonic crystals", *Phys. Rev. B*, **57**, pp. 2841-2848, 1998.
- [5] R. L. Sutherland, V. P. Tondiglia, L. V. Natarajan, S. Chandra, "Switchable orthorhombic F photonic crystals formed by holographic polymerization-induced phase separation of liquid crystal", *Optics Express*, **10**, pp. 1074-1082, 2002.
- [6] K. Sakoda, "Optical Properties of Photonic Crystals", Springer, Berlin, 2001.
- [7] J. D. Joannopoulos, R. D. Meade, J. N. Winn, "Molding the Flow of Light", Princeton University Press, 1995.
- [8] K. M. Ho, C. T. Chan, and, C. M. Soukoulis, "Existence of a Photonic Gap in Periodic Dielectric Structures", *Phys. Rev. Lett.*, **65**, pp. 3152-3155, 1990.
- [9] S. G. Johnson, and J. D. Joannopoulos, "Block-iterative frequency-domain methods for Maxwell's equations in a planewave basis", *Opt. Express*, **8**, pp. 173-190, 2001.
- [10] R. D. Meade, A. M. Rappe, K. D. Brommer, J. D. Joannopoulos, and O. L. Alerhand, "Accurate theoretical analysis of photonic band-gap materials", *Phys. Rev. B*, **48**, pp. 8434-8437, 1993.
- [11] H. S. Sözüer, J. W. Haus, and R. Inguva, "Photonic bands: Convergence problems with the plane-wave method", *Phys. Rev. B*, **45**, pp. 13962-13972, 1992.
- [12] D. Hermann, M. Frank, K. Busch and P. Wölffe, "Photonic band structure computations", *Opt. Express*, **8**, pp. 167-172, 2001.
- [13] K. Ohtaka, T. Ueta, and K. Amemiya, "Calculation of photonic bands using vector cylindrical waves and reflectivity of light for an array of dielectric rods", *Phys. Rev B*, **57**, pp. 2550-2568, 1998.
- [14] C. T. Chan, Q. L. Yu, and K. M. Ho, "Order-N spectral method for electromagnetic waves", *Phys. Rev B*, **51**, pp. 16 635-16 642, 1995.
- [15] M. Qui and S. He, "A non-orthogonal finite-difference time-domain method for computing the band structure of a two-dimensional photonic crystal with dielectric and metallic inclusions", *J. Appl. Phys.*, **87**, pp. 8268-8275, 2000.
- [16] J. B. Pendry and A. MacKinnon, "Calculation of Photon Dispersion Relations", *Phys. Rev. Lett.*, **69**, pp. 2772-2775, 1992.
- [17] W. Axmann and P. Kuchment, "An efficient finite element method for computing spectra of photonic and acoustic band-gap materials", *J. Comput. Phys.*, **150**, pp. 468-481, 1999.

- [18] P. A. Knipp, and T. L. Reinecke, "Boundary-element calculations of electromagnetic band-structure of photonic crystals", *Physica E*, **2**, pp. 920-924, 1998.
- [19] Ch. Hafner, "Post-modern Electromagnetics Using Intelligent Maxwell Solvers", John Wiley & Sons, 1999.
- [20] Ch. Hafner, "MaX-1: A visual electromagnetics platform", John Wiley & Sons, 1998.
- [21] P. R. Villeneuve and M. Piche, "Photonic band gaps in two-dimensional square and hexagonal lattices", *Phys. Rev. B*, **46**, pp. 4969-4972, 1992.
- [22] M. Plihal and A. A. Maradudin, "Photonic band structure of two-dimensional systems: the triangular lattice", *Phys. Rev. B*, **44**, pp. 8565-8571, 1991.
- [23] Ch. Hafner, J. Smajic, The Computational Optics Group Web Page (IFH, ETH Zurich), <http://alphard.ethz.ch/>.
- [24] I. N. Vekua, "New methods for solving elliptic equations", North-Holland, Amsterdam, 1967.
- [25] G. H. Golub and C. F. Van Loan, "Matrix Computations", John Hopkins University Press, Baltimore, 1996.
- [26] F. G. Bogdanov, D. D. Karkashadze, and R. S. Zaridze, in "Generalized Multipole Techniques for Electromagnetic and Light Scattering", edited by T. Wriedt, pp. 143-172, Elsevier, Amsterdam, 1999.
- [27] K. Sakoda, N. Kawai, T. Ito, A. Chutinan, S. Noda, T. Mitsuyu, and K. Hirao, "Photonic bands of metallic systems. I. Principle of calculation and accuracy", *Phys. Rev. B*, **64**, pp. 045116, 2001.
- [28] E. Moreno, D. Erni and Ch. Hafner, "Band structure computations of metallic photonic crystals with the multiple multipole method", *Phys. Rev. B*, **65**, pp. 155120: 1-10, 2002.
- [29] S. G. Johnson and J. D. Joannopoulos, The MIT Photonic-Bands Package home page, <http://ab-initio.mit.edu/mpb/>.
- [30] R. D. Meade, K. D. Brommer, A. M. Rappe and J. D. Joannopoulos, "Photonic band states in periodic dielectric materials", *Phys. Rev. B*, **44**, pp. 13 772 - 13 774, 1991.
- [31] E. Moreno, D. Erni and Ch. Hafner, "Modeling of discontinuities in photonic crystal waveguides with the multiple multipole method", *Phys. Rev. B*, **66**, pp. 036618, 2002.



**Jasmin Smajic** was born in Tuzla, Bosnia and Herzegovina, in 1971. He received a Dipl. El.-Ing. degree from Faculty of Electrical Engineering, Tuzla in 1996. Since 1996 he has been working at the Faculty of Electrical Engineering in Tuzla on numerical calculation of electromagnetic field, numerical mathematics and optimization. He got a M.Sc. degree in 1998 from the Faculty of Electrical Engineering and Computing in Zagreb, Croatia, for the analysis of magnetic field in non-linear material. He received a Ph.D. in 2001 from Faculty of Electrical Engineering and Computing in Zagreb, Croatia, for numerical calculation of time-varying field in non-linear material and electrical machine design optimization. Since 2002 he is a postdoctoral research fellow in the Computational Optics group of the Laboratory for Electromagnetic Fields and Microwave Electronics at the ETH Zurich. His current research interest includes numerical field calculation and design optimization of photonic crystal devices.



**Christian Hafner** was born in Zurich, Switzerland, in 1952. He received a Dipl. El.-Ing. Degree, Doctoral Degree, and Venia Legendi from Swiss Federal Institute of Technology (ETH), Zürich in 1975, 1980, and 1987 respectively. In 1999 he was given the title of Professor. Since 1976 he has been working at the ETH on the development of methods for computational electromagnetics and for optimization problems. He has developed the Multiple Multipole Program (MMP), the MaX-1 package, the Generalized Genetic Programming (GGP) code, and various optimization codes. He worked on various applications (electrostatics, EM scattering, antenna, waveguides and waveguide discontinuities, gratings, chiral media, etc.). His current focus is on photonic crystals, microstructured optical fibers, and Scanning Nearfield Optical Microscopes (SNOM). In 1990 he obtained the second prize of the Seymour Cray award for scientific computing and in 2001 he has been awarded the 2000 Outstanding Journal Paper Award by the Applied Computational Electromagnetics Society. He is member of the Electromagnetics Academy.



**Daniel Erni** was born in Lugano, Switzerland, in 1961. He received an El.-Ing. HTL degree from Interkantonales Technikum Rapperswil HTL in 1986, and a Dipl. El.-Ing. degree from Swiss Federal Institute of Technology (ETH), Zürich in 1990, both in electrical engineering. Since 1990 he has been working at the Laboratory for Electromagnetic Fields and Microwave Electronics (ETH) on nonlinear wave propagation, laser diode modeling (multi-section DFB and DBR lasers, VCSELs), computational electro-magnetics and on the design of non-periodic optical waveguide gratings e.g. by means of evolutionary algorithms.

He got a Ph.D. degree in 1996 for the investigation of non-periodic waveguide gratings and non-periodic coupled cavity laser concepts. His current research interests include highly multimode optical signal transmission in optical interconnects (i.e. in optical backplanes with extremely large waveguide cross sections) as well as alternative waveguiding concepts for dense integrated optical devices like e.g. photonic crystal devices, couplers and WDM filter structures. In 2001 he has been awarded the 2000 Outstanding Journal Paper Award by the Applied Computational Electromagnetics Society for a contribution on the application of evolutionary optimization algorithms in computational optics. Dr. Erni is the head of the Communication Photonics Group at ETH Zurich ([www.photonics.ee.ethz.ch](http://www.photonics.ee.ethz.ch)). He is also a member of the Swiss Physical Society (SPS), of the German Physical Society (DPG), of the Optical Society of America (OSA), and of the IEEE.